INTERFACE

royalsocietypublishing.org/journal/rsif

Research

Cite this article: Sheppard S, Dikicioglu D. 2019 Dynamic modelling of the killing mechanism of action by virus-infected yeasts. *J. R. Soc. Interface* **16**: 20190064.
http://dx.doi.org/10.1098/rsif.2019.0064

Received: 1 February 2019
Accepted: 21 February 2019

Subject Category:
Life Sciences–Engineering interface

Subject Areas:
biotechnology, systems biology

Keywords:
killer yeast, dynamic model, toxin, apoptosis, K1/K2, K28

Author for correspondence:
Duygu Dikicioglu
e-mail: dd345@cam.ac.uk

Electronic supplementary material is available online at https://dx.doi.org/10.6084/m9.figshare.c.4421270.

THE ROYAL SOCIETY PUBLISHING

Dynamic modelling of the killing mechanism of action by virus-infected yeasts

Sean Sheppard[1] and Duygu Dikicioglu[2]

[1]St John's College, St John's Street, Cambridge, UK
[2]Department of Chemical Engineering and Biotechnology, University of Cambridge, Cambridge, UK

DD, 0000-0002-3018-4790

Killer yeasts are microorganisms, which can produce and secrete proteinaceous toxins, a characteristic gained via infection by a virus. These toxins are able to kill sensitive cells of the same or a related species. From a biotechnological perspective, killer yeasts are beneficial due to their antifungal/antimicrobial activity, but also regarded as problematic for large-scale fermentation processes, whereby those yeasts would kill starter cultures species and lead to stuck fermentations. Here, we propose a mechanistic model of the toxin-binding kinetics pertaining to the killer population coupled with the toxin-induced death kinetics of the sensitive population to study toxic action. The dynamic model captured the transient toxic activity starting from the introduction of killer cells into the culture at the time of inoculation through to induced cell death. The kinetics of K1/K2 activity via its primary pathway of toxicity was 5.5 times faster than its activity at low concentration inducing the apoptotic pathway in sensitive cells. Conversely, we showed that the primary pathway for K28 was approximately three times slower than its equivalent apoptotic pathway, indicating the particular relevance of K28 in biotechnological applications where the toxin concentration is rarely above those limits to trigger the primary pathway of killer activity.

1. Background

Killer yeasts are eukaryotic, single-celled fungi, which produce and secrete toxic proteins that are lethal to sensitive cells; the phenomenon was first characterized in 1963 [1]. Several yeast species are recognized as possessing the killer characteristic with the most extensively studied being *Saccharomyces cerevisiae* [2]. The potential of killer yeasts due to their antimicrobial activity has been explored widely, especially within the context of applications in the food industry [3]. Although being acknowledged as a promising premise for a number of biotechnological applications, killer activity of yeasts is also deemed undesirable on other platforms.

These infected cells are often detected in wine fermentation processes whereby killer yeasts contaminate starter cultures, killing the microbiological fermenting agents. Ratios as low as one killer yeast for every hundred sensitive yeasts was reported to eliminate the starter culture population within 24 h [4–6]. Stuck fermentations, which are characterized by high concentrations of acetaldehyde and lactic acid, are often a consequence and are typical of a very distasteful wine product [7]. Wineries can incur substantial financial losses due to stuck fermentations, and therefore, killer yeasts are considered an important concern compromising success in commercial wine processing [8]. Early research on wine microbial communities focused on devising control strategies to manage killer yeasts in wine fermentation in order to reduce the chance of spoilage [2]. More recently, the possibility of commercializing killer yeasts in wine fermentation specifically due to their antifungal activity was also investigated [9]. Within this remit, genetic modification techniques were

explored as potential tools for constructing wine yeast strains, which are resistant to, and/or possess the killer factor [10]. Starter cultures, into which these strains would successfully be integrated, could assist the control and prevention of contaminating fungal species via the production of toxins, making wine production more reliable than before, and reducing the costs associated with stuck fermentations substantially [11,12].

Killer yeast systems are classified on the basis of the molecular characteristics of their toxins, the variations in the encoding genetic determinants, the presence or the lack of cross-immunity, and their killing profiles [13]. *Saccharomyces cerevisiae* is by far the most studied yeast species with regard to acquired toxic activity, with four distinct toxin proteins characterized (K1, K2, K28 and Klus), thus it contributes vastly to our understanding of killer yeasts and their infecting viruses. The virus, L-A, is an icosahedral double stranded (ds) RNA virus of the yeast *S. cerevisiae* with a single 4.6 kb genomic segment that encodes its major coat protein, Gag (76 kDa) and a Gag-Pol fusion protein (180 kDa) formed by a-1 ribosomal frameshift, which encode an RNA-dependent RNA polymerase. A number of satellite dsRNAs, called M dsRNAs, encoding a secreted protein toxin and immunity to that toxin are hosted in separate viral particles, whose replication and encapsidation are supported by L-A. Each toxin is encoded by a single open reading frame and is synthesized as a polypeptide preprotoxin. The preprotoxin comprises a hydrophobic amino terminus representative of secretion and is modified via the endoplasmic reticulum and the Golgi apparatus of the host for activation of the toxin prior to its secretion [8,14–17].

Only those yeasts that possess both the M dsRNAs and L-A, are able to produce effective toxins. Although the transmission of L-A and M from cell to cell occurs exclusively during the mating process but not via natural release from the cell or entry by another mechanism, it is the high frequency of yeast mating, which ensures the wide distribution of these viruses in natural isolates. Moreover, the structural and the functional similarities of these viruses to dsRNA viruses of mammalian systems evoke further interest in their study [14,17,18].

K1 comprises α- (9.5 kDa) and β-subunits (9.0 kDa) [13]. The β-subunit is responsible for receptor binding to sensitive cells, and the α-subunit induces the lethal effect. K2 structurally resembles K1 with subunits that are only marginally larger than those of K1 [19], despite substantial differences in the sequences of their dsRNA, their molecular weights, isoelectric points and optimum pH [20]. The mechanisms through which these toxin proteins kill susceptible cells display some level of variance, although striking similarities also exist. K2 toxin, less extensively characterized than K1, was accepted to have a similar mechanism of action to K1, apart from some differences that occur at the plasma membrane and cell wall level. The patterns of processing of both killer proteins by the sensitive cells were also reported to be similar. Despite the similarities of their toxins, K1 and K2 killer strains were reported to be able to kill each other even though they are immune to their own toxin [21]. K28 is also secreted as a heterodimer of α- (10.5 kDa) and β-subunits (11 kDa) [22]. The mechanism of K28-induced lethality was reported to be significantly different than that of K1-induced lethality [23]. Klus was recently isolated as a novel toxin produced by *S. cerevisiae* [24,25], and its toxic action is not yet well understood.

Cells that are susceptible to these toxins were identified to possess two different types of sites or receptors that bind the killer toxin with different affinities [26]. The first step of K1/K2 binding was reported as the low affinity, high velocity, energy independent adsorption of the killer toxin on β-1,6-D-glucans embedded in the cell wall [27,28]. Once bound, the toxin had a high affinity, low velocity, energy-dependent interaction with Kre1p receptors, which are glycosyl-phosphatidylinositol-linked glycoproteins located on the cell membrane [29,30]. Subsequently, the α-subunit of the toxin was shown to trigger the formation of voltage-independent cation transmembrane channels, which would then cause the leakage of H^+ and K^+ ions, followed by cell death [31]. In contrast to K1 or K2, K28 was reported to initially bind to α-1,3-linked mannose residues of a 185-kDa cell wall mannoprotein [32]. The toxin would then interact with the Erd2p receptor triggering toxin uptake into the cytosol by receptor-mediated endocytosis [33]. The β-subunit of K28 would be ubiquitinated and proteasomally degraded following the toxin's uptake and retrograde transport through the Golgi and endoplasmic reticulum to the cytosol, while the α-subunit cleaved from its β-subunit and migrated into the sensitive cell's nucleus [34]. There the lethal subunit would arrest cell cycle at the G1/S boundary, preventing the separation of the daughter and the mother cells, effectively killing both cells [34,35] (figure 1).

The primary mechanisms of action for these toxins are in place at high concentrations of toxin availability. A secondary mechanism was described relatively recently and was shown to be in effect upon medium to low-concentration exposure to toxins. The toxin proteins were shown to induce programmed cell death at concentrations that were not sufficient to trigger the primary action pathways [11,36–39]. The affected sensitive cells were shown to enter an apoptotic state; exhibiting markers such as DNA fragmentation, chromatin condensation and phosphatidylserine externalization [38]. The activation of the yeast metacaspase 1 (Yca1p) via toxins would eventually yield to the release of reactive oxygen species, triggering a cascade of events consigning the cell to death via apoptosis [40,41]. This response appears to be universally induced at low concentrations, irrespective of the nature of the toxin protein in question. Toxic action via programmed cell death has been proposed as the predominant mechanism by which killer yeasts kill sensitive species in natural environments where they are found in much lower concentrations [42].

The secondary mechanism of toxic action, the oxidative route was implicated to have high killing potential, and thus play an important role along with the apoptotic route. However, the threshold at which the switch between the primary and the secondary mechanisms occur, or the relationship between the toxin binding kinetics and the toxin-induced death kinetics are still unknown. How the sensitive and killer members of the same species reach equilibrium is still an unanswered question, too. In this work, we built a deterministic model that could simulate both the toxic activity of killer cells, and the toxin-induced damage on the sensitive population upon exposure. The model equipped us with a novel platform to (i) study the toxic effects of killer yeasts on sensitive populations, (ii) predict how the system responds to varying levels of toxin and (iii) develop strategies to control and contain killer population and maintain the survival of the sensitive population.

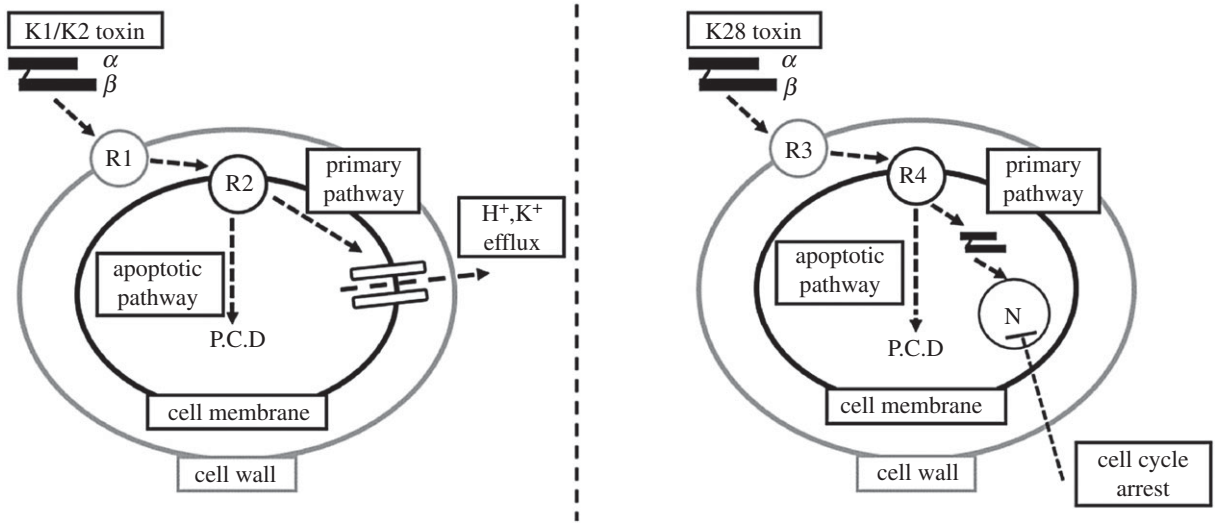

Figure 1. Schematic diagram of the toxin action pathways for K1, K2 and K28. Each toxin either induces cell death via the primary or apoptotic pathway depending on concentration. K1 and K2 share a common pathway and mechanistic action and K28 has its own unique pathway. The abbreviations used are as follows: P.C.D, programmed cell death; N, nucleus; R1, β-1,6-D-glucans; R2, Kre1p receptor; R3, α-1,3-linked mannose residues; R4, Erd2p receptor.

We selected both the killer and the susceptible population to be comprising *S. cerevisiae* and compiled the extensive qualitative and quantitative data available in the literature on the kinetic action of the K1, K2 and K28 toxins at high and low concentrations. We implemented a model structure and verified the models' predictive power on independent datasets; they were able to accurately match empirical data. We then employed the models to gain in-depth novel insight into how the mechanisms for toxic activity changed in response to the extent of toxin exposure. The constructed models are publicly available via EBI's BioModels Database [43] via access nos.: MODEL1804230001 and MODEL1804230002 for K1/2 and K28, respectively.

2. Material and methods

2.1. Model structure and modelling platform

The model described the killer toxin activity, which comprised the binding phase of the toxin to the cell wall and membrane, and the sensitive cell activity, which comprised toxin-induced death of the sensitive fraction of the population. These activities explaining the mechanism were represented by chemical reactions between molecular species and the dynamics were governed by rate laws associated with each reaction. The model was built using ordinary differential equations. The model was built and simulated in the open-source software COPASI 4.22 (Build 170) [44]. The timescale of the analysis was measured in minutes as it allowed the observation of both the rapid toxin binding, and the relatively slow toxin-induced death in the same frame. The concentration of both the toxins and cells were represented as the number of molecules per millilitre (molecules/ml).

2.2. Experimental data

Experimental data were acquired from relevant publications. Whenever data were only presented in the form of figures in their respective publications, the open-source Java platform Plot Digitizer 2.6.8 (http://plotdigitizer.sourceforge.net/) was employed to get an accurate estimate of the raw data.

The specific masses of the toxins were acquired from [13] as 19 000 Da for K1, 21 500 Da for K2 and 21 500 Da for K28; consequently, 1 pg of toxin equated to 3.125×10^{-7}, 2.8×10^{-7} and 2.8×10^{-7} molecules of K1, K2 and K28, respectively. Data from *Pichia membranifaciens* PMKT and PMKT2 toxins, which were reported to be analogous to K1 and K28, were employed to infer kinetic information and to complement data on *S. cerevisiae* toxins when no direct data were available [11,45,46]. Experiments from which data were collected were carried out under the ideal conditions for each toxin and so the same conditions are assumed to exist for the model. There was an overlap of the optimal temperature and pH for all three toxins, and all data employed in the study were reported at the same conditions of pH = 4.7 and $T = 22^{\circ}C$ [31,47,48]. The analysis was conducted on the assumption of a fixed-sized viable cell population where a dynamic equilibrium between the natural death and growth rates was assumed to hold, in order to detect the extent of death caused by the toxins.

2.3. Representation of the toxin binding phase

The main underlying assumption of the binding model was that it assumed a well-mixed population of sensitive cells. Toxin proteins were also assumed to be well-mixed within sensitive cells, so there was no heterogeneity regarding how toxins would bind to individual cells, but instead would accumulate simultaneously across all cells in the population; 16 800 000 molecules of K1 were calculated to saturate the cell wall receptors of a single *S. cerevisiae* cell from the data provided in [26]. The cell membrane Kre1p receptor was reported to be saturated at a concentration 50-fold lower than that needed to saturate the cell wall receptor [27], yielding a saturation constant of 336 000 molecules. The kinetics of K1 binding to the cell membrane was reported to be 6.333 times slower than binding to the cell wall [26]. Kinetic data for cell wall and cell membrane binding were available for K1 and K2 (table 1), but not for K28. However, the number of cell wall mannoproteins was reported to be similar to that of β-1,6-D-glucans [49] and K28 has a similar mass to K1 and K2. The saturation constants, cell wall and cell membrane binding rates were assumed as identical, since no data were available to contradict this assumption. Furthermore, the binding rate of PMKT2 (K28 equivalent toxin) to α-1,3-linked mannose residues was reported to have similar kinetics to K1 [11], providing further support for the assumption made.

2.4. Representation of toxin-induced cell death

An individual *S. cerevisiae* cell of average sensitivity was reported to be killed by at least 28 000 K1 or K28 molecules [27,50], which was selected as the threshold value for the activation of the

Table 1. Kinetics of toxin cell wall binding.

toxin protein	toxin concentration (molecules/cell)	time to bind 50% of molecules (min)	time until binding rate plateaus (min)	reference
K1	56 400	0.88	10	[26]
K1	1600	1.1	10	[26]
K2	1000	0.9	10	[28]

Table 2. Kinetics of toxin-induced cell death. LU, lethal units.

pathway	toxin protein	toxin concentration (molecules/cell)	time to kill 50% of population (min)	time to kill 98% of population (min)	reference
primary	K1	75 000	7	40	[35]
apoptotic	K1	2600	40	220	[38]
primary	K28	9.63×10^9	100	560	[35,51]
primary	K28	3.75×10^6	90	560	[35,51]
apoptotic	K28	2800	40	230	[38]
primary	PMKT2	28 000	120	570	[11]

primary pathway. Below this concentration (28 000 molecules/cell), the model activated the secondary apoptotic pathway, as was reported earlier [38]. Toxin-induced cell death was reported to be ineffective at toxin concentration of 852 K1 molecules/cell and 1080 K28 molecules/cell [38]. The threshold at which the cells displayed the first signs of apoptotic cell death upon exposure to toxin was adopted from the investigation of PMKT2 activity, where, at this threshold, approximately 35% of the cells showed signs of entering apoptosis after 90 min upon toxin exposure, with the ratio rising to 95% after 180 min [11]. A similarity was assumed between the K1/2- and K28-induced cell death kinetics due to the now well-acknowledged similarities between the mechanisms of toxic action to induce apoptotic cell death. Kinetic data for toxin-induced death were available for both K1 and K28, but only at certain concentration levels (table 2).

Statistical inference studies on population cell death were conducted by carrying out maximum likelihood estimation running on MATLAB R2018b (Mathworks). The average fraction of the dead population was determined at the 20th minute post exposure to toxin by fitting a logarithmic function to the death kinetics provided for K1 and K28 in the event of primary or apoptotic cell death in table 2. This information was employed as prior knowledge about normally distributed populations of cells. The maximum-likelihood estimates on the fraction of population affected were determined for population sizes ranging from 50 to 5×10^7 cells, noting that cell counts ranging from 10^5 to 10^7 are standard for a typical yeast population. The fractional difference between the likelihood estimates and the given *a priori* knowledge were used to evaluate how valid the predictions would be for populations of varying sizes.

3. Results

A single model structure was employed to describe K1/K2 kinetics and K28 kinetics, with relevant constants to account for the difference in rates of toxin binding and toxin-induced cell death (see table 3 for constants). A modular system of toxin binding and killing activities was implemented, and the model complexity was increased in a stepwise manner such that the final working model either made use of (during reconstruction) or explained (during benchmarking and validation) virtually all of the empirical data available to date.

3.1. Molecular crowding around cell wall receptors impedes binding at high toxin abundance

A common binding model proposing similar binding mechanisms for K1 and K28 was constructed, as suggested by empirical data reported in previous studies, and the rate of binding of the toxin on the yeast cell wall was captured by parameter estimation from [26]. Binding of the toxin molecules on the cell wall receptors and on the cell membrane was modelled separately. The simplest preliminary model for binding was constructed only to account for the phenomenon occurring on the cell wall. Michaelis–Menten kinetics, often employed to quantify the degree of interaction between a ligand and a receptor population [52], was selected for this model (equation (3.1)), but it failed to capture the initial dynamics of cell wall binding, overestimating the amount of toxin bound (figure 1). This simple model did not account for any crowding of toxin molecules at the receptor binding sites, and therefore allowed binding without any constraints as long as unbound toxins were available. Consequently, the possibility of any potential competition at the receptor binding sites, which could slow binding down by restricting access to the receptors despite their availability was overruled in this initial model.

$$\frac{\delta[\text{Cell Wall}_{\text{Toxin}}]}{\delta t} = \frac{(V\text{max}_{\text{CW}} \times [\text{Unbound}_{\text{Toxin}}])}{(K_{\text{CW}} + [\text{Unbound}_{\text{Toxin}}])}. \quad (3.1)$$

In order to account for this inefficiency in binding, the rate law was modified to equation (3.2), improving the simulation of the binding characteristics observed during the first 2 min following the exposure of sensitive cells to toxin molecules (figure 2*a*). This improvement suggested that a potential interaction between the unbound toxin molecules and those that were already bound to the cell wall receptors could indeed hinder binding within the initial minutes upon

Table 3. Parameters of the rate equations used as the basis of the model.[a]

biological process	parameter	value	units
cell wall binding	$kcat_{CW}$	1.23	1/min
cell wall binding	K_{CW}	9.07×10^9	molecules/l
cell membrane binding	$kcat_{CM}$	0.205	1/min
cell membrane binding	K_{CM}	9.07×10^9	molecules/l
toxin-induced cell death via primary pathway (K1 and K28)	$LU_{Primary}$	28 000	LU
toxin-induced cell death via apoptotic pathway (K1)	$LU_{Apoptotic(K1)}$	825	LU
toxin-induced cell death via apoptotic pathway (K28)	$LU_{Apoptotic(K28)}$	1080	LU
K1-induced death	$k_{TID(K1)}$	5.0×10^{-7}	l · min/molecules
K28-induced death	$k_{TID(K28)}$	2.5×10^{-13}	l · min/molecules
adjusted K1-induced death	$k_{ATID(K1)}$	2.5×10^{-9}	l · min/molecules
K1-induced apoptosis	$k_{TIA(K1)}$	4.0×10^{-9}	l · min/molecules
K28-induced apoptosis	$k_{TIA(K28)}$	5.0×10^{-9}	l · min/molecules
K1-triggered apoptotic death	$k_{AD(K1)}$	0.30	l · min/molecules
K28-triggered apoptotic death	$k_{AD(K28)}$	0.30	l · min/molecules

[a]If the value of a parameter was obtained by parameter scanning, the median value is displayed above.

exposure. The standard Hill equation proposes an alternative kinetic form to capture the cooperativity of binding and was originally selected by the authors to describe the binding kinetics. However, the predictions made by the model employing the derived form of equation (3.2) was shown to predict the empirical data more successfully than the Hill equation derivate, and therefore the form presented below was adopted in the final model structure.

$$\frac{\delta[\text{Cell Wall}_{\text{Toxin}}]}{\delta t} = \frac{(\text{kcat}_{\text{CW}} \times ([\text{Unbound}_{\text{Toxin}}])^2)}{(K_{\text{CW}} + [\text{Unbound}_{\text{Toxin}}])}. \quad (3.2)$$

The saturation of the cell surface receptors was described by a saturation constant such that if the concentration of bound toxin was higher than the value of that constant, no further binding would take place (equation (3.3)). This allowed the representation of a step-wise binding process that was dependent on the availability of toxin molecules per each cell.

$$\frac{\delta[\text{Cell Wall}_{\text{Toxin}}]}{\delta t} = \begin{cases} \dfrac{[\text{Cell Wall}_{\text{Toxin}}]}{\text{Viable Cells}} < 1.68 \times 10^7, & \dfrac{(\text{kcat}_{\text{CW}} \times ([\text{Unbound}_{\text{Toxin}}])^2)}{(K_{\text{CW}} + [\text{Unbound}_{\text{Toxin}}])} \\ \text{else}, & 0 \end{cases}. \quad (3.3)$$

This model of cell wall binding kinetics was simulated for an arbitrarily selected population of 1×10^7 susceptible cells that were exposed to varying initial concentrations of unbound toxins in order to investigate the effect of saturation on cell wall binding kinetics. The initial concentration of unbound toxins varied in a 100-fold range. The analysis showed that as long as the saturation of the receptors on the cell wall was avoided, the binding kinetics remained constant (figure 1*b*). Similar binding rates were reported in experiments where the initial unbound toxin concentration was varied by more than 50-fold, providing further support for these findings [26,28].

The cell wall binding kinetics for toxin molecules was extended also to describe cell membrane binding kinetics. Although the membrane binding mechanism was assumed to be similar to the mechanism for binding the cell wall, the rate constant of binding, $kcat_{CM}$, was reported to be 6.333 times slower [26]. The saturation of the cell membrane surface by the toxins was also described by a conditionality, and the final model for binding accounted for the unbound toxin molecules to initially bind to the cell wall receptors (represented in equation (3.4)), and then to be translocated to the cell membrane (represented in equation (3.5)).

The model predicted that the extent of toxin binding to the cell wall rapidly increased and reached a maximum of 56 000 molecules/cell 103 s after the initial exposure to the

$$\frac{\delta[\text{Cell Wall}_{\text{Toxin}}]}{\delta t} = \begin{cases} \dfrac{[\text{Cell Wall}_{\text{Toxin}}]}{\text{Viable Cells}} < 1.68 \times 10^7, & \dfrac{(\text{kcat}_{\text{CW}} \times ([\text{Unbound}_{\text{Toxin}}])^2)}{(K_{\text{CW}} + [\text{Unbound}_{\text{Toxin}}])} \\ \text{else}, & 0 \end{cases} - \begin{cases} \dfrac{[\text{Cell Membrane}_{\text{Toxin}}]}{\text{Viable Cells}} < 3.36 \times 10^5, & \dfrac{(\text{kcat}_{\text{CM}} \times ([\text{Cell Wall}_{\text{Toxin}}])^2)}{(K_{\text{CM}} + [\text{Cell Wall}_{\text{Toxin}}])} \\ \text{else}, & 0 \end{cases} \quad (3.4)$$

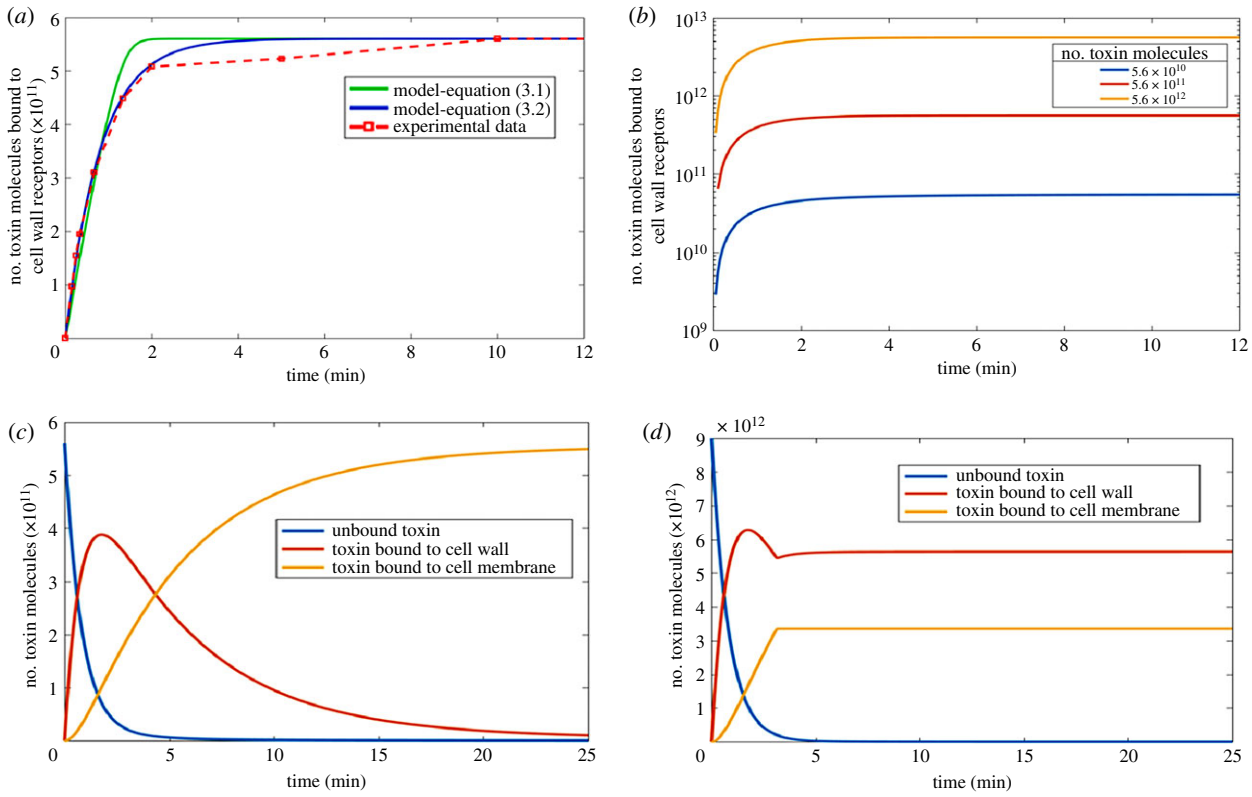

Figure 2. Binding kinetics of toxin molecules. (*a*) Kinetic models of cell wall binding of toxins employing equation (3.1) shown in green and equation (3.2) shown in blue. Experimental data shown in red (data points connected with a dashed line) was taken from [26]. Initial population of unbound toxins was fixed at 5.6×10^{11} molecules. (*b*) Simulations using the kinetic model for cell wall binding of toxin molecules (equation (3.3)) starting from different initial concentrations of unbound toxins. The initial unbound toxin concentration was explored across a range of 2 orders of magnitude. (*c*) Predictive model simulations explaining the kinetics of K1, K2 and K28 binding to the cell wall and the cell membrane with unsaturated receptors available on both surfaces. The initial toxin availability was 5.6×10^4 molecules/cell. (*d*) Predictive model simulations explaining the kinetics of K1, K2 and K28 binding to the cell wall and the cell membrane with receptors on both surfaces reaching full saturation. The initial toxin availability was 9×10^5 molecules/cell. Note that the total number of toxin molecules for 1×10^7 susceptible cells are displayed in (*a–d*). Information on creating the figure from model simulations are detailed in electronic supplementary material, S4. (Online version in colour.)

and
$$\frac{\delta[\text{Cell Membrane}_{\text{Toxin}}]}{\delta t} = \begin{cases} \dfrac{[\text{Cell Membrane}_{\text{Toxin}}]}{\text{Viable Cells}} < 3.36 \times 10^5, & \dfrac{(\text{kcat}_{\text{CM}} \times ([\text{Cell Wall}_{\text{Toxin}}])^2)}{(K_{\text{CM}} + [\text{Cell Wall}_{\text{Toxin}}])} \\ \text{else}, & 0 \end{cases}. \quad (3.5)$$

toxin proteins. This bound toxin population was observed to shrink later, as toxin molecules slowly migrated towards the surface of the cell membrane. Toxin migration to the cell membrane was observed slow down after approximately 20 min leading towards the saturation of the membrane surface (figure 2*c*). The membrane receptor population was shown to fully saturate at a toxin concentration of 336 000 molecules/cell or higher, and no further toxin molecule movement was observed from the cell wall to the membrane, and two distinct toxin populations bound to different compartments of the cell were achieved (figure 2*d*).

3.2. Integrating toxin-induced death dynamics and toxin binding dynamics via the utilization of lethality units

The model representing the kinetics of toxin binding to the cell wall and the cell membrane was further extended to represent the dynamics of cell death in a sensitive population exposed to toxins released by the killer population. A functional link was established between the toxin molecules and the cells that were doomed to die upon exposure to these molecules in order to facilitate the reconstruction of an integrated model. A new measure called the lethal unit (LU) was introduced into the model in order to represent a cluster of toxin molecules, which would be sufficient to induce toxin-associated death of a single yeast cell. The two different routes of toxin-induced death; via the primary pathway or via the apoptotic pathway required differently sized clusters of toxin molecules to be defined into a single LU. Therefore, the number of toxin molecules initially available per cell was used by the model to determine the pathway through which the toxins exerted their lethal effect. If the initial concentration was above 28 000 toxin molecules/cell, the model adopted the primary pathway of toxin activity to induce cell death by converting every 28 000 molecules into a single LU. Otherwise, 852 or 1080 toxin molecules leading

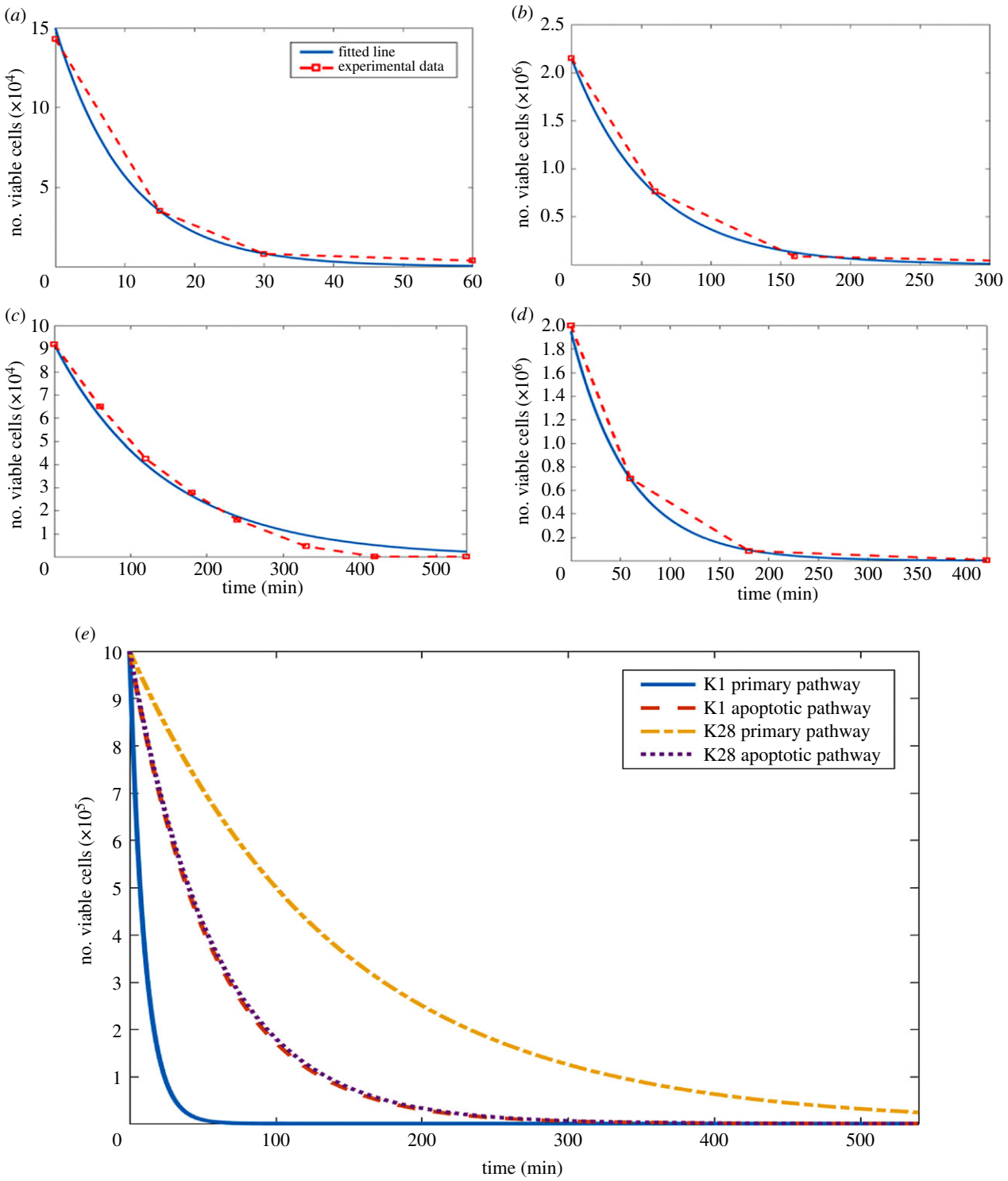

Figure 3. Simulation of toxin-induced cell death. (*a*,*b*) Kinetic models of toxin-induced cell death by K1 for the primary pathway of toxin activity (*a*) and the apoptosis-inducing pathway of toxin activity (*b*). Experimental data shown in red (data points connected with a dashed line) was taken from [38]. Parameter estimation was employed to fit the data. Toxin concentration was 75 000 molecules/cell in (*a*) and 2600 molecules/cell in (*b*). (*c*,*d*) Kinetic models of toxin-induced cell death by K28 for the primary pathway of toxin activity (*c*) and the apoptosis-inducing pathway of toxin activity (*d*). Experimental data shown in red (data points connected with a dashed line) was taken from [38,51]. Parameter estimation was employed to fit the data. Toxin concentration was 9.63×10^9 molecules/cell in (*c*) and 2800 molecules/cell in (*d*). The original data points employed in parameter estimation (*a*–*d*) are provided as electronic supplementary material, S5. (*e*) Comparison of the kinetics of the toxin-induced cell death pathways for K1 and K28 are provided with the initial size of the viable population normalized to 150 000 for all four pathways. Information on creating the figure from model simulations are detailed in electronic supplementary material, S4. (Online version in colour.)

the sensitive cell towards apoptosis were employed to represent a single LU for K1 and K28, respectively

$$\left\{\begin{array}{l} 28\,000\ \mathrm{Unbound}_{\mathrm{Toxin}} \rightarrow 1\ \mathrm{LU}_{\mathrm{Primary}} \\ 825\ \mathrm{Unbound}_{\mathrm{Toxin}} \rightarrow 1\ \mathrm{LU}_{\mathrm{Apoptotic\ (K1)}} \\ 1080\ \mathrm{Unbound}_{\mathrm{Toxin}} \rightarrow 1\ \mathrm{LU}_{\mathrm{Apoptotic\ (K28)}} \end{array}\right\}. \tag{3.6}$$

The efficacy of the toxins on the cell population was described by mass action kinetics. The cell death kinetics via the apoptotic pathway and the primary pathway of toxin activity were thus compared for both K1 and K28. Our model simple mass action kinetic analysis showed that K1 introduced at a concentration of 75 000 molecules/cell,

killed off 50% of the sensitive population in 7 min. In 40 min, 98% of the whole population was dead (figure 3*a*). The apoptosis-inducing toxin lethality acted considerably slower on the sensitive cells than the primary route of toxic activity. The presence of K1 at a concentration of 2600 molecules/cell could only kill 50% of the population after 40 min post initial toxin exposure, while it took as long as 220 min (greater than 3.5 h) for 98% of the cells constituting the population to become inviable (figure 3*b*).

K28 had a substantially slower primary effect to induce cell death than K1 did. The data showed that nearly 100 min was needed to reduce the viable cell population by 50% even at a toxin concentration as high as 9.63×10^9 molecules/cell. More than 560 min was required for 98% of the cell population to become inviable (figure 3*c*). By contrast, the apoptotic pathway for K28 was nearly as fast as that for K1 to induce cell death, and in fact, the pertaining kinetics were even faster than those for its primary pathway. The availability of 2800 K28 molecules/cell was sufficient to kill 50% of the population within 40 min, and 98% of the population was inviable after 230 min post exposure to toxin (figure 3*d*).

The rates of toxin-induced death displayed a nearly 16-fold difference across different toxins available at different concentrations. The apoptotic pathways of K1 and K28 were very similar, inducing death in 1.763% and 1.713% of the population per minute, respectively. This similarity, despite the substantial differences in the kinetic activity shown by their primary pathways, supported the hypothesis that toxin-induced apoptotic cell death could indeed be a universal mechanism of toxin activity (figure 3*e*). The primary pathway of K1 induced death 15.8-fold faster than that of K28, killing 0.613% and 9.687% of the population per minute, respectively.

3.3. Integrated model of the primary pathway of toxic action

The integration of the binding models with the killing models for K1 and K28 necessitated the introduction of a single parameter, whose activity could be traced across both stages of binding followed by killing. In order to build the integrated model of toxin binding and toxin-induced death, the binding equations needed to be modified such that the binding was modelled based not on individual toxin molecules but on a cluster of toxin molecules represented by a single LU. In terms of the constants of the equation, this modification affected the saturation constants. Once a single LU was bound to the cell membrane, it was assumed to induce cell death subsequently, and the same LU was used up in the killing model to convert a viable cell into an inviable one. In this system, both K1 and K28 were considered to be used only once, being bound on to the cell wall, and then on to the membrane, followed by its binding to the DNA. The toxin-induced cell death dynamics were represented by the following mass action kinetics in equations (3.7) and (3.8) for K and K28, respectively.

$$\frac{\delta[\text{Viable}_{\text{Cell}}]}{\delta t} = -\left(k_{\text{ATID(K1)}} \times ([\text{Viable}_{\text{Cell}}])^{1.5} \times [\text{Kre1p}_{\text{Toxin (K1)}}]\right) \tag{3.7}$$

and

$$\frac{\delta[\text{Viable}_{\text{Cell}}]}{\delta t} = -\left(k_{\text{TID(K28)}} \times [\text{Viable}_{\text{Cell}}] \times [\text{Erd2p}_{\text{Toxin (K28)}}]\right). \tag{3.8}$$

Kre1p and Erd2p are the respective cell membrane receptors of K1 and K28, and toxin bound receptor concentration represented the last step of the binding phase mechanism. $[\text{Viable}_{\text{Cell}}]$ represented the size of the population of sensitive cells. $[\text{Kre1p}_{\text{Toxin(K1)}}]$ and $[\text{Erd2p}_{\text{Toxin(K28)}}]$ represented the amount of K1 and K28 molecules bound to their respective receptors. The second order rate constant for toxin-induced death, k_{TID}, was determined by parameter optimization.

The models of both K1 and K28 toxins successfully simulated toxin-induced death dynamics reported earlier by [38,51] (figure 4*a*,*b*). The initial dynamics observed in the empirical data indicated faster cell death when the number of viable cells was higher for K1. Possibly, the high cell numbers could specifically facilitate the binding of an LU-equivalent number of toxin molecules to Kre1p with reduced competition. As the population of viable cells decreased, the ability for unbound K1 molecules to find a viable cell to bind to decreased accordingly. In order to achieve a model that could represent this phenomenon, the order of the rate equation with respect to the viable cell concentration was set as 1.5 (equation (3.7)), allowing rapid K1 killer activity from toxin binding on the cell wall and the cell membrane to the cell death. This modification was not needed for the case of K28, indicating K1's superior efficiency in toxic activity, particularly during the initial period of the population's exposure to toxins.

3.4. Integrated model of the apoptotic pathway of toxic action

Programmed cell death upon exposure to a low concentration of toxins could be deemed a two-stage process where an LU equivalent of toxin molecules bind to the cell membrane receptors triggering apoptosis, followed by cell death. Although the fate of the cell has already been determined at the initial stage, apoptosis requires a set of controlled actions to take place, introducing a time delay before the cells consigned to death can actually be considered as inviable. We presented this phenomenon in the model by introducing an additional model step to mark when cells would be considered as apoptotic. It represents the first stage of apoptosis described above, where the cells start showing signs of programmed cell death, and therefore are consigned to die, but are not technically dead yet. Toxins were modelled to induce cell death following a mass action rate law when at least a single LU equivalent of toxin molecules were bound to the cell membrane receptors, as in modelling of the primary toxin action pathway. The fate determination and death for K1 and K28 binding were represented by equations (3.9) and (3.10) and equations (3.11) and (3.12), respectively.

$$\frac{\delta[\text{Apoptotic}_{\text{Cell}}]}{\delta t} = k_{\text{TIA(K1)}} \times [\text{Viable}_{\text{Cell}}] \times [\text{Kre1p}_{\text{Toxin (K1)}}], \tag{3.9}$$

$$\frac{\delta[\text{Inviable}_{\text{Cell}}]}{\delta t} = k_{\text{AD(K1)}} \times [\text{Apoptotic}_{\text{Cell}}] \times [\text{Kre1p}_{\text{Toxin (K1)}}], \tag{3.10}$$

$$\frac{\delta[\text{Apoptotic}_{\text{Cell}}]}{\delta t} = k_{\text{TIA(K28)}} \times [\text{Viable}_{\text{Cell}}] \times [\text{Erd2p}_{\text{Toxin (K28)}}] \tag{3.11}$$

and

$$\frac{\delta[\text{Inviable}_{\text{Cell}}]}{\delta t} = k_{\text{AD(K28)}} \times [\text{Apoptotic}_{\text{Cell}}] \times [\text{Erd2p}_{\text{Toxin (K28)}}], \tag{3.12}$$

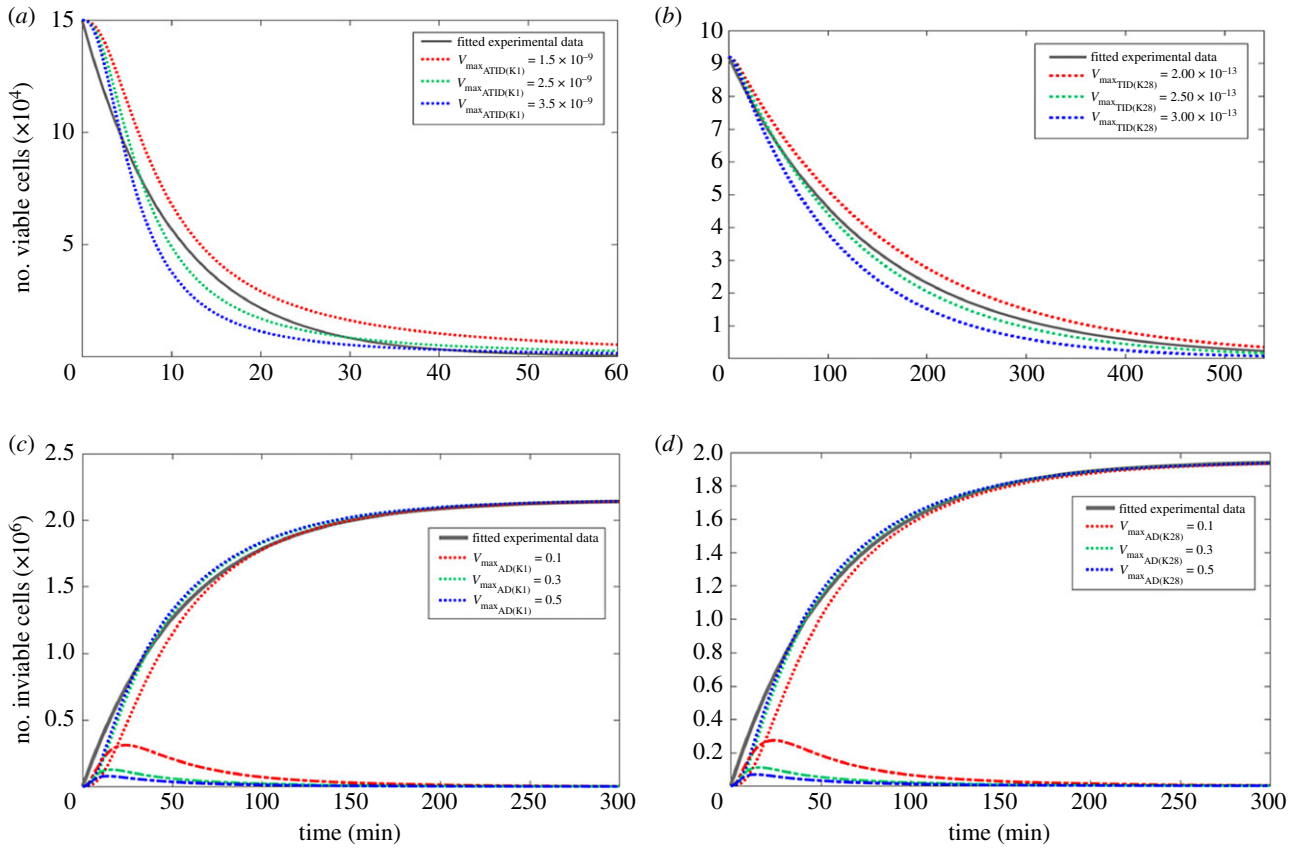

Figure 4. Modelling of the primary and secondary mechanisms of toxin-induced death. (*a*,*b*) Kinetic models of toxin-induced cell death via the primary action pathway for K1 (*a*) and K28 (*b*). The simulations were carried out using different maximum specific rate of cell death constants. The experimental data displayed in the grey solid line was adapted from [38,51]. The model employed equation (3.7) for (*a*) and equation (3.8) for (*b*). The total (bound + unbound) K1 concentration is 75 000 toxin molecules/cell, and the total K28 concentration was 9.63×10^9 toxin molecules/cell. (*c*,*d*) Kinetic models of toxin-induced cell death via the apoptotic action pathway for K1 (*c*) and K28 (*d*). The experimental data displayed in the grey solid line was adopted from [38]. The model employed equations (3.9) and (3.10) for (*c*) and equations (3.11) and (3.12) for (*d*). The dotted lines indicated the simulations concerning the inviable population, whereas the dashed lines denoted the fraction of the population that entered the apoptotic phase, but did not yet emerge as dead cells in (*c*) and (*d*). The toxin concentration necessary to induce death in a single cell is 2600 molecules in (*c*) and 2800 molecules in (*d*). All simulations were carried out using different maximum specific rate of cell death constants, and the simulations that used increasing values are shown in red to green to blue dashed lines in (*a*–*d*). Information on creating the figure from model simulations are detailed in electronic supplementary material, S4. (Online version in colour.)

k_{TIA} was determined via parameter estimation from [11] by identifying the duration for a cell that was exposed to 2800 PMKT2 molecules to displayed recognized apoptotic signals. The loss of viability was predicted successfully for both K1 and K28 (figure 4*c*,*d*). The initial killer activity of the model suggested a lag period before toxin-induced death was observed, which was likely to be missed in experiments due to incompatibility of the timescales. Experimental investigations to date focused on monitoring cell death over long timescales and have failed to sample the population within the first couple of minutes upon toxin exposure. The model simulations were able to capture the delayed response in the early dynamics of the response. The transition from the apoptotic state to cell death was predicted to take place rather quickly by the model, as shown by the dynamic profile of the size of this intermediary population (figure 4*c*,*d*). Furthermore, a large variation in the second order rate constant of death did not have a substantial impact on the dynamics of toxin-induced death, suggesting that the rate at which apoptosis was triggered in the sensitive cell population was the important step in this process. This further implied limited heterogeneity within the population as to how long apoptotic processes would take to kill the cell.

3.5. Modelling the killer activity of K1 and K28 toxins on sensitive populations of the same species

Generalized models of the killer toxin activity on sensitive yeasts were developed for two well-known killer toxins virally acquired by yeasts with distinct mechanisms of action, K1 and K28. Different stages and relevant design concerns discussed in the sections above were used to reconstruct a modular global model and were then specialized for K1 and K28 activity accordingly. The different constants optimized and estimated for K1 and K28 from empirical data, which used in their respective models, are presented in table 3.

The different modules were brought together under two conservation laws, leading to the final working models for simulating K1 and K28 activity: the total number of toxin molecules bound and unbound to receptors remained constant throughout the simulation, and the sensitive yeast population maintained steady growth, with natural death of the cells to replace the newly formed daughter cells, thus keeping the mean number and the mean size of the cells as well as the mean number of receptor molecules on cell wall and on the cell membrane constant unless exposed to killer toxins. These models were created and simulated using the open-source COPASI software, and the constructed models were made

available both as electronic supplementary material, S1 and S2. They were also deposited in the BioModels database with the following identifiers; MODEL1804230001 and MODEL1804230002 for K1 and K28, respectively.

4. Discussion

We constructed a deterministic model, which predicted the killing dynamics of K1and K28 toxins, which agrees with the existing empirical data. Since the dynamics of K1 and K28 toxic activity was not investigated comparatively before, our model provided a useful platform to conduct a comparative analysis of the kinetics of these toxins and their efficacy. The fastest toxic activity was observed in response to K1 availability at high concentrations, when the primary toxin pathway was employed, and this was 5.5 times faster than its action when the apoptotic pathway was induced. Conversely, the route of action through the K28 primary pathway was approximately three times slower than the route of action via its apoptotic pathway. K1 available at high concentrations was more effective in killing the sensitive cell population than K28, when the primary pathways of toxicity were in order. However, the kinetics of the apoptotic pathways were essentially equivalent for both K1and K28. The large variability in the K28 primary pathway could be due to the fact K28 arrests cells specifically at the G1/S boundary phase of cell replication [11]. The rate at which cells enter the G1/S boundary phase would depend on environmental conditions and the state of the cell culture [53]. Therefore, varying experimental conditions across different datasets exploring K28 toxic activity would have led to these differing results.

Killer toxins are unable to kill all the sensitive cells within a population [54]. Although it would be less likely to expect such 'unresponsiveness' in an ecosystem, within a minutes time frame, although the fraction of cells that is not responsive to the killer yeasts within longer time frames would indicate that it is highly likely that death of 98% of the sensitive population could never be achieved. This time frame would naturally vary across different toxins, although the lack of empirical data does not allow testing of this phenomenon using these models. Nevertheless, the death of 98% of the population has been routinely achieved in the laboratory environment, with extensive empirical data made available. Such data have been employed in this study, and our models successfully predicted the behaviour of the population under such conditions in the light of these existing empirical data.

The binding dynamics of the model showed that as long as the bound toxin concentration did saturate the surface receptors, the rate at which molecules adsorbed on the cell surface was independent of toxin concentration. Model predictions showed that the binding kinetics of the K28 primary pathway and that of PMKT2, the analogous toxin produced by *P. membranifaciens* were similar despite large differences in the available concentration of the two toxins, indicating that toxin-induced death was governed by the binding of a single LU-equivalent of toxin molecules and that further increasing the amount of toxin bound did not necessarily speed up the rate of the process.

The empirical data on toxin binding, however, was largely disparate across different reports. Kurzweilová *et al*. reported that 16 800 000 molecules of K1 could bind to a single cell's wall [26]. Recently, a modest figure of 555 K1 molecules/cell was proposed [28]. The number of β-1,6-D-glucans on a haploid parent yeast cell wall was estimated to vary in the range of 6 600 000–11 000 000 [27,55] and would be even higher for diploid cells than these reported here. Considering that a single toxin molecule can bind to any of these primary receptors, which are available most of the time, binding data reported by Kurzweilová *et al*. provided better representation of the binding kinetics for K1 than more recent reports did in the model simulations, which complemented the other empirical data, particularly on the mechanism of action of the apoptotic pathway.

K1 toxin was long disputed also to interact with the outward-rectifier potassium channel of the plasma membrane, Tok1p in addition to the Kre1p membrane receptor [56]. A counterargument was proposed by Breinig *et al*. proposing that Tok1p channels were only activated downstream, once K1 had already triggered ionophoric disruption [30]. The binding dynamics proposed by the model support the hypothesis that the Tok1p channels would be activated downstream along the toxin-induced death pathway rather than at the initial binding stage.

Several aspects of design were important for modelling the killer toxin dynamics. The total number of toxin molecules available, both bound to a receptor and unbound, was assumed to be constant according to the main conservation law. This conservation was built on two assumptions: the half-life of the killer toxins exceeded that of the simulation period, so that the effect of toxin protein degradation could be excluded. Although the authors are not aware of the availability of such data for *S. cerevisiae* K1, K2 or K28, a study on a *Schwanniomyces occidentalis* killer protein, which displayed 75% identity and 83% similarity with killer toxin K2, was reported to have a half-life of at least 8 h at 30°C at pH 4.4 [57]; at a sufficiently close environment to those of optimal yeast cultivations. Since the stability of K2 toxin depended substantially on the environmental conditions, available data [58] should be consulted in conducting the analysis and evaluating the findings under the assumption of different environmental conditions. The second assumption was on the killer yeast population being maintained at a steady rate, thus not introducing excess toxic proteins into the environment, as was discussed earlier. Furthermore, the toxin export through efflux pumps, and the binding equilibrium of toxin to receptors in the cell wall and the plasma membrane were excluded from the model, since there is no evidence yet in support of potential resistance mechanisms to be active against killer toxins. However, as more empirical data becomes available on binding equilibria, these models can flexibly be extended to include the rates of association and dissociation of these molecules with the surface receptors. We conducted a sensitivity analysis to investigate this notion further, and tested how the primary mechanism and apoptotic cell death were affected by changing the binding rate of the K1 toxin on the cell wall surface. Increasing the binding kinetics by three orders of magnitude only affected the time the toxin molecules took to reach the maximum extent of binding on the cell wall glucans, reducing it down from *ca* 1.5 min to nearly instantaneous response. Slowing down the cell wall binding kinetics, on the other hand, extended the time it took the system to reach a steady state, as would have been expected. Interestingly, the fraction of

cells affected by the apoptotic mechanism was 21% higher as the primary cell wall binding kinetics slowed down by 2–3 orders of magnitude. This indicated a preference of the system to shift from the primary towards the apoptotic mechanism of action, as the cell wall binding kinetics of the primary mechanism, which was the initial step in the process, was forced to become limiting even further. Concurrently reducing the membrane binding kinetics by three orders of magnitude increased the concentration of the toxin-bound cell wall glucans, but did not have any effect on the primary or the apoptotic mechanisms.

Another important feature considered at the integration stage was the possibility of the recycling of toxin molecules. The notion of being able to reutilize toxin molecules, possibly similar to what the cell does in the case of the currency metabolites, was evaluated as a potential strategy. However, once passed through the nuclear membrane, K1 and K28 were reported to bind the DNA irreversibly [59], also undergoing an irreversible structural modification. Furthermore, no reports existed on the possibility of any reuse of toxins, and this notion was thus excluded from the design. Density of the cell culture, nutrient availability and dispersal were all shown to affect the competitive ability of toxin-producing yeasts [60,61], therefore, these parameters would potentially need to be taken into consideration for specific applications.

A distinct threshold of the initial concentration of toxin molecules available per cell was adopted in this model to determine whether the toxic effect would be exerted via the primary or apoptotic pathway. Although this threshold was very useful for comparing and contrasting the kinetics of these two pathways of toxic activity and represented the real kinetics of these mechanisms sufficiently well in the light of existing empirical data, it should also be noted that simultaneous activity of the primary and the apoptotic pathways was also reported across a range of toxin concentrations; K1 was shown to kill cells via both the primary and apoptotic pathway in a range of concentrations varying from 28 000 to 3000 toxin molecules/cell, but a 'breaking point' between the two mechanisms was also reported in the same work at around 7500 molecules/cell where the pathway rapidly switched from one pathway to the other [38]. The flexibility of the constructed models would allow the relevant modifications to be made to tailor the time and concentration dependence of killer toxin activity, if further experimental evidence backed up the transitional nature of these two mechanisms of action within proposed ranges of concentration profiles.

A stable killer phenotype has been known to necessitate a coordinated action by a group of host chromosomal genes including SEC genes, required for general secretion of extracellular proteins and glycoproteins, the KEX-encoded proteases for preprototoxin processing and precursor maturation of the yeast pheromone α-factor, in addition to a set of chromosomal genes, which either directly or indirectly affect dsRNA virus propagation, classified into two major groups; the maintenance of killer genes, MAK, and the superkiller genes, SKI [62]. The detailed mechanisms of action pertaining to these are beyond the scope of the work here and were thus excluded from the models constructed in this work.

The initial phase of toxin-induced death simulated by the model was observed to be consistently different from empirical observations, where a short lag phase was observed in model simulations introduced due to the binding of toxins prior to cell death, which was not observed experimentally. This discrepancy was thought to be caused by either of the two following reasons, or the combination thereof: (i) the deterministic nature of the model, which assumed synchronous action for all members of the cell population, failed to represent the heterogeneity caused by spatial or stochastic variations in actual systems; and (ii) the most commonly employed experimental technique used in measuring cell death kinetics involves taking aliquots from the cell culture to measure the toxin activity at specific time points. It is quite common not to sample the culture within the first 15 min upon exposure and, therefore, the experimental data available could just be an artefact of extrapolation as the true kinetics were not recorded during this time period. The model predictions, in fact, may provide the missing details on the initial kinetics of cell death.

The deterministic models constructed here are valid when dealing with a large number of cells. The model constants employed here were based on data collected from *in vitro* studies, where a well-mixed volume of a large number of cells was investigated. However, in real ecosystems, the role of stochasticity would be more prominent than in these 'created' environments. Since these models could simulate the behaviour of how an average cell would behave, they overlook the possibility of the behaviour of individual cells being very different and highly variant. To test this notion, maximum likelihood estimates were determined for the population and the fraction of the population that would be killed upon toxin exposure for different population size ranging from 50 to 5×10^7. The difference in the fraction of population killed as a function of population size showed an asymmetric distribution, with a skew (i.e. a bias) towards estimating a lower fraction of the population to be killed than what *in vitro* studies reported to be valid for the population average. This observation was highly prominent in small population sizes of 50 to 5000 cells. Furthermore, the results indicated that the behaviour of individual cells could not be predicted for small populations, since our analysis showed that the estimates could be off by as much as 60%. By contrast, the difference was so low (less than 1%) for large populations of 5×10^5 or more cells that, in practice, it could safely be assumed that the empirical data collected from *in vitro* studies would be valid for average cells from large yeast populations (electronic supplementary material, S3). One important thing to note would be that in our analysis, neither different toxin types nor death by different mechanisms of action could be classified into statistically meaningful clusters. Therefore, although we observed very clear effects of stochasticity in small populations, which would indicate limited predictability of cell fate at the individual cell level, the observations we made did not further contribute to the current understanding of the differences between cellular mechanisms of action or toxin types.

The action of cell membrane binding of K28 is complex as the toxin does not simply bind to the cell periphery and trigger downstream effects. Instead, the toxin is endocytosed into the cell's cytoplasm where it undergoes extensive modification before it can exert lethality in the cell's nucleus. The mechanism of the pathway and most of the intracellular modifications taking place are now well-understood, albeit without any kinetic information available

[18]. Therefore, all post-binding processes were lumped into the equations representing toxin-induced death in the current version of the model. Availability of kinetic data on this mechanism would allow the reconstruction and implementation of a more detailed model describing the physiology of toxin binding and cell death. The model of binding proposed in this work was nevertheless able to predict the overall killer activity of K28 successfully, however, it lacks sufficient details on the mechanistic action, which could only be implemented in the light of future empirical kinetic data.

In this work, we investigated the K1 and K28 toxin killing mechanisms of action in a dynamic model that incorporates toxin-binding kinetics. We determined the relevant kinetic rules and the kinetic rate constants, through which the overall reaction kinetics observed and reported in the literature could successfully be captured. The models proposed here are the first of their kind in representing a direct killing mechanism and an indirect apoptosis inducing mechanism in conjunction and showed that the K1/K2 toxins and the K28 toxins were not only effective via different mechanisms of action, but also they displayed different dynamics. Since the kinetics of K1 and K28 toxins were not investigated in a consistent experimental set-up, which would allow comparable data to be generated, the testing of our findings on the differences in dynamics yet remains a challenge to be confirmed empirically. The models of killer toxin activity constructed here are able to simulate how the dynamics of sensitive yeast populations are affected by exposure to different toxins at various concentrations, enabling us to simulate excess environments as well as mildly toxic environments, which would be more likely to be encountered in the wild. These models (BioModels Database [43], MODEL1804230001 for K1 and MODEL1804230002 for K28) constitute a useful platform to explore the dynamics of toxic activity and to offer insights into the mechanisms and suitability of each toxin and pathway for managing starter cultures. The predictions achieved from such models could be used to predict optimal ratios of killer and sensitive yeast cells and propose control actions to maintain these optimal ratios. Accurate quantitative frameworks achieved through such models may assist building resilient and productive starter cultures of mixed fungal and yeast species for different biotechnological applications.

Data accessibility. All research data pertaining this work are provided in the electronic supplementary material. The models are also available through EBI's Biomodels Database (MODEL1804230001 and MODEL1804230002).

Authors' contributions. D.D. designed and supervised the work. S.S. performed the modelling analysis. S.S. and D.D. drafted the manuscript. Both authors read and approved the final manuscript.

Competing interests. The authors declare that they have no conflict of interest.

Funding. This work was supported by the Leverhulme Trust and the Isaac Newton Trust (ECF-2016-681 to D.D.).

Acknowledgements. The authors would like to thank Louise Bartle from the University of Adelaide for discussions on the role of killer yeasts in wine fermentations.

References

1. Bevan EA. 1963 The physiological basis of the killer character in yeast. In *Proc. 11th Int. Congr. Genet, The Hague, The Netherlands, September*, pp. 202–203. Oxford, UK: Pergamon Press.
2. Young TW, Yagiu M. 1978 A comparison of the killer character in different yeasts and its classification. *Antonie Van Leeuwenhoek* **44**, 59–77. (doi:10.1007/BF00400077)
3. Cappelli A *et al.* 2014 A *Wickerhamomyces anomalus* killer strain in the malaria vector *Anopheles stephensi*. *PLoS ONE* **9**, e95988. (doi:10.1371/journal.pone.0095988)
4. Pérez F, Ramírez M, Regodón JA. 2001 Influence of killer strains of *Saccharomyces cerevisiae* on wine fermentation. *Antonie Van Leeuwenhoek* **79**, 393–399. (doi:10.1023/A:1012034608908)
5. Maturano YP, Nally MC, Toro ME, Castellanos de Figueroa LI, Combina M, Vazquez F. 2012 Monitoring of killer yeast populations in mixed cultures: influence of incubation temperature of microvinifications samples. *World J. Microbiol. Biotechnol.* **28**, 3135–3142. (doi:10.1007/s11274-012-1123-1)
6. Satyanarayana T, Kunze G (eds). 2017 *Yeast diversity in human welfare*. Singapore: Springer.
7. Carrau FM, Neirotti E, Gioia O. 1993 Stuck wine fermentations: effect of killer/sensitive yeast interactions. *J. Ferment. Bioeng.* **76**, 67–69. (doi:10.1016/0922-338X(93)90056-E)
8. Van Vuuren HJJ, Jacobs CJ. 1992 Killer yeasts in the wine industry: a review. *Am. J. Enol. Viticult.* **43**, 119–128.
9. Yap NA, de Barros Lopes M, Langridge P, Henschke PA. 2000 The incidence of killer activity of non-*Saccharomyces* yeasts towards indigenous yeast species of grape must: potential application in wine fermentation. *J. Appl. Microbiol.* **89**, 381–389. (doi:10.1046/j.1365-2672.2000.01124.x)
10. Seki T, Choi EH, Ryu D. 1985 Construction of killer wine yeast strain. *Appl. Environ. Microbiol.* **49**, 1211–1215.
11. Santos A, Alonso A, Belda I, Marquina D. 2013 Cell cycle arrest and apoptosis, two alternative mechanisms for PMKT2 killer activity. *Fungal Genet. Biol.* **50**, 44–54. (doi:10.1016/j.fgb.2012.10.006)
12. de Ullivarri MF, Mendoza LM, Raya RR. 2014 Killer activity of *Saccharomyces cerevisiae* strains: partial characterization and strategies to improve the biocontrol efficacy in winemaking. *Antonie Van Leeuwenhoek* **106**, 865–878. (doi:10.1007/s10482-014-0256-7)
13. Magliani W, Conti S, Gerloni M, Bertolotti D, Polonelli L. 1997 Yeast killer systems. *Clin. Microbiol. Rev.* **10**, 369–400. (doi:10.1128/CMR.10.3.369)
14. Patton JT. 2008 *Segmented double-stranded RNA viruses: structure and molecular biology*. Caister Academic Press. See https://www.caister.com/rnav.
15. Bostian KA, Hopper JE, Rogers DT, Tipper DJ. 1980 Translational analysis of the killer-associated virus-like particle dsRNA genome of *S. cerevisiae*: M dsRNA encodes toxin. *Cell* **19**, 403–414. (doi:10.1016/0092-8674(80)90514-0)
16. Rodríguez-Cousiño N, Esteban R. 2017 Relationships and evolution of double-stranded rna totiviruses of yeasts inferred from analysis of L-A-2 and L-BC variants in wine yeast strain populations. *Appl. Environ. Microbiol.* **83**, e02991–16. (doi:10.1128/AEM.02991-16)
17. Ribas JC, Wickner RB. 1998 The Gag domain of the Gag-Pol fusion protein directs incorporation into the L-A double-stranded RNA viral particles in *Saccharomyces cerevisiae*. *J. Biol. Chem.* **273**, 9306–9311. (doi:10.1074/JBC.273.15.9306)
18. Becker B, Schmitt M. 2017 Yeast killer toxin K28: biology and unique strategy of host cell intoxication and killing. *Toxins (Basel)* **9**, 333. (doi:10.3390/toxins9100333)
19. Dignard D, Whiteway M, Germain D, Tessier D, Thomas DY. 1991 Expression in yeast of a cDNA copy of the K2 killer toxin gene. *Mol. Gen. Genet.* **227**, 127–136. (doi:10.1007/BF00260717)
20. Pfeiffer P, Radler F. 1984 Comparison of the killer toxin of several yeasts and the purification of a toxin of type K2. *Arch. Microbiol.* **137**, 357–361. (doi:10.1007/BF00410734)
21. Novotna D, Flegelova H, Janderova B. 2004 Different action of killer toxins K1 and K2 on the plasma membrane and the cell wall of

Saccharomyces cerevisiae. *FEMS Yeast Res.* **4**, 803–813. (doi:10.1016/j.femsyr.2004.04.007)

22. Schmitt MJ, Tipper DJ. 1990 K28, a unique double-stranded RNA killer virus of *Saccharomyces cerevisiae*. *Mol. Cell. Biol.* **10**, 4807–4815. (doi:10.1128/MCB.10.9.4807)
23. Breinig F, Sendzik T, Eisfeld K, Schmitt MJ. 2006 Dissecting toxin immunity in virus-infected killer yeast uncovers an intrinsic strategy of self-protection. *Proc. Natl Acad. Sci. USA* **103**, 3810–3815. (doi:10.1073/pnas.0510070103)
24. Melvydas V, Bružauskaitė I, Gedminienė G, Šiekštelė R. 2016 A novel *Saccharomyces cerevisiae* killer strain secreting the X factor related to killer activity and inhibition of *S. cerevisiae* K1, K2 and K28 killer toxins. *Ind. J. Microbiol.* **56**, 335–343. (doi:10.1007/s12088-016-0589-1)
25. Rodríguez-Cousiño N, Maqueda M, Ambrona J, Zamora E, Esteban R, Ramírez M. 2011 A new wine *Saccharomyces cerevisiae* killer toxin (Klus), encoded by a double-stranded RNA virus, with broad antifungal activity is evolutionarily related to a chromosomal host gene. *Appl. Environ. Microbiol.* **77**, 1822–1832. (doi:10.1128/AEM.02501-10)
26. Kurzweilov H, Sigler K. 1994 Kinetic studies of killer toxin K1 binding to yeast cells indicate two receptor populations. *Arch. Microbiol.* **162**, 211–214. (doi:10.1007/BF00314477)
27. Bussey H, Saville D, Hutchins K, Palfree RG. 1979 Binding of yeast killer toxin to a cell wall receptor on sensitive *Saccharomyces cerevisiae*. *J. Bacteriol.* **140**, 888–892.
28. Lukša J, Podoliankaitė M, Vepštaitė I, Strazdaitė-Žielienė Ž, Urbonavičius J, Servienė E. 2015 Yeast β-1,6-glucan is a primary target for the *Saccharomyces cerevisiae* K2 toxin. *Eukaryot. Cell* **14**, 406–414. (doi:10.1128/EC.00287-14)
29. Breinig F, Schleinkofer K, Schmitt MJ. 2004 Yeast Kre1p is GPI-anchored and involved in both cell wall assembly and architecture. *Microbiology* **150**, 3209–3218. (doi:10.1099/mic.0.27175-0)
30. Breinig F, Tipper DJ, Schmitt MJ. 2002 Kre1p, the plasma membrane receptor for the yeast K1 viral toxin. *Cell* **108**, 395–405. (doi:10.1016/S0092-8674(02)00634-7)
31. Martinac B, Zhu H, Kubalski A, Zhou XL, Culbertson M, Bussey H, Kung C. 1990 Yeast K1 killer toxin forms ion channels in sensitive yeast spheroplasts and in artificial liposomes. *Proc. Natl Acad. Sci. USA* **87**, 6228–6232. (doi:10.1073/pnas.87.16.6228)
32. Schmitt M, Radler F. 1987 Mannoprotein of the yeast cell wall as primary receptor for the killer toxin of *Saccharomyces cerevisiae* strain 28. *Microbiology* **133**, 3347–3354. (doi:10.1099/00221287-133-12-3347)
33. Becker B *et al*. 2016 H/KDEL receptors mediate host cell intoxication by a viral A/B toxin in yeast. *Sci. Rep.* **6**, 31105. (doi:10.1038/srep31105)
34. Schmitt MJ, Breinig F. 2006 Yeast viral killer toxins: lethality and self-protection. *Nat. Rev. Microbiol.* **4**, 212–221. (doi:10.1038/nrmicro1347)
35. Schmitt M, Brendel M, Schwarz R, Radler F. 1989 Inhibition of DNA synthesis in *Saccharomyces cerevisiae* by yeast killer toxin KT28. *Microbiology* **135**, 1529–1535. (doi:10.1099/00221287-135-6-1529)
36. Ivanovska I, Hardwick JM. 2005 Viruses activate a genetically conserved cell death pathway in a unicellular organism. *J. Cell Biol.* **170**, 391–399. (doi:10.1083/jcb.200503069)
37. Klassen R, Meinhardt F. 2005 Induction of DNA damage and apoptosis in *Saccharomyces cerevisiae* by a yeast killer toxin. *Cell. Microbiol.* **7**, 393–401. (doi:10.1111/j.1462-5822.2004.00469.x)
38. Reiter J, Herker E, Madeo F, Schmitt MJ. 2005 Viral killer toxins induce caspase-mediated apoptosis in yeast. *J. Cell Biol.* **168**, 353–358. (doi:10.1083/jcb.200408071)
39. Schmitt MJ, Reiter J. 2008 Viral induced yeast apoptosis. *Biochim. Biophys. Acta Mol. Cell Res.* **1783**, 1413–1417. (doi:10.1016/J.BBAMCR.2008.01.017)
40. Hamann A, Brust D, Osiewacz HD. 2008 Apoptosis pathways in fungal growth, development and ageing. *Trends Microbiol.* **16**, 276–283. (doi:10.1016/j.tim.2008.03.003)
41. Mazzoni C, Falcone C. 2008 Caspase-dependent apoptosis in yeast. *Biochim. Biophys. Acta Mol. Cell Res.* **1783**, 1320–1327. (doi:10.1016/j.bbamcr.2008.02.015)
42. Starmer WT, Lachance M-A. 2011 Yeast ecology. In (eds CP Kurtzman, JW Fell, T Boekhout) *The yeasts, a taxonomic study*, 5th edn, pp. 65–83. Amsterdam, The Netherlands: Elsevier.
43. Chelliah V *et al*. 2015 BioModels: ten-year anniversary. *Nucleic Acids Res.* **43**, D542–D548. (doi:10.1093/nar/gku1181)
44. Hoops S *et al*. 2006 COPASI—a COmplex PAthway SImulator. *Bioinformatics* **22**, 3067–3074. (doi:10.1093/bioinformatics/btl485)
45. Belda I, Ruiz J, Alonso A, Marquina D, Santos A. 2017 The biology of *Pichia membranifaciens* killer toxins. *Toxins (Basel)* **9**, 112. (doi:10.3390/toxins9040112)
46. Santos A, Marquina D, Leal JA, Peinado JM. 2000 (1→6)-β-D-Glucan as cell wall receptor for *Pichia membranifaciens* killer toxin. *Appl. Environ. Microbiol.* **66**, 1809–1813. (doi:10.1128/AEM.66.5.1809-1813.2000)
47. Petering JE, Symons MR, Langridge P, Henschke PA. 1991 Determination of killer yeast activity in fermenting grape juice by using a marked *Saccharomyces* wine yeast strain. *Appl. Environ. Microbiol.* **57**, 3232–3236.
48. Baeza ME, Sanhueza MA, Cifuentes VH. 2008 Occurrence of killer yeast strains in industrial and clinical yeast isolates. *Biol. Res.* **41**, 173–182. (doi:10.4067/S0716-97602008000200007)
49. Lipke PN, Ovalle R. 1998 Cell wall architecture in yeast: new structure and new challenges. *J. Bacteriol.* **180**, 3735–3740.
50. Palfree RGE, Bussey H. 1979 Yeast killer toxin: purification and characterisation of the protein toxin from *Saccharomyces cerevisiae*. *Eur. J. Biochem.* **93**, 487–493. (doi:10.1111/j.1432-1033.1979.tb12847.x)
51. Schmitt MJ, Klavehn P, Wang J, Schonig I, Tipper DJ. 1996 Cell cycle studies on the mode of action of yeast K28 killer toxin. *Microbiology* **142**, 2655–2662. (doi:10.1099/00221287-142-9-2655)
52. Attie AD, Raines RT. 1995 Analysis of receptor-ligand interactions. *J. Chem. Educ.* **72**, 119–124. (doi:10.1021/ed072p119)
53. Seaton DD, Krishnan J. 2016 Model-based analysis of cell cycle responses to dynamically changing environments. *PLoS Comput. Biol.* **12**, e1004604. (doi:10.1371/journal.pcbi.1004604)
54. Wickner RB. 1979 The killer double-stranded RNA plasmids of yeast. *Plasmid* **2**, 303–322. (doi:10.1016/0147-619X(79)90015-5)
55. Klis FM, de Koster CG, Brul S. 2014 Cell wall-related bionumbers and bioestimates of *Saccharomyces cerevisiae* and *Candida albicans*. *Eukaryot. Cell* **13**, 2–9. (doi:10.1128/EC.00250-13)
56. Ahmed A, Sesti F, Ilan N, Shih TM, Sturley SL, Goldstein SA. 1999 A molecular target for viral killer toxin: TOK1 potassium channels. *Cell* **99**, 283–291. (doi:10.1016/S0092-8674(00)81659-1)
57. Chen WB, Han YF, Jong SC, Chang SC. 2000 Isolation, purification, and characterization of a killer protein from *Schwanniomyces occidentalis*. *Appl. Environ. Microbiol.* **66**, 5348–5352. (doi:10.1128/AEM.66.12.5348-5352.2000)
58. Lukša J, Serva S, Servienė E. 2016 *Saccharomyces cerevisiae* K2 toxin requires acidic environment for unidirectional folding into active state. *Mycoscience* **57**, 51–57. (doi:10.1016/J.MYC.2015.08.003)
59. Eisfeld K, Riffer F, Mentges J, Schmitt MJ. 2000 Endocytotic uptake and retrograde transport of a virally encoded killer toxin in yeast. *Mol. Microbiol.* **37**, 926–940. (doi:10.1046/j.1365-2958.2000.02063.x)
60. Greig D, Travisano M. 2008 Density-dependent effects on allelopathic interactions in yeast. *Evolution (N.Y)* **62**, 521–527. (doi:10.1111/j.1558-5646.2007.00292.x)
61. Wloch-Salamon DM, Gerla D, Hoekstra RF, de Visser JAGM. 2008 Effect of dispersal and nutrient availability on the competitive ability of toxin-producing yeast. *Proc. R. Soc. Lond. B* **275**, 535–541. (doi:10.1098/rspb.2007.1461)
62. Schmitt MJ, Breinig F. 2002 The viral killer system in yeast: from molecular biology to application. *FEMS Microbiol. Rev.* **26**, 257–276. (doi:10.1111/j.1574-6976.2002.tb00614.x)